DREAM Interrupted: Severing LIN-35-MuvB association in *Caenorhabditis elegans* impairs DREAM function but not its chromatin localization

Paul D. Goetsch[*,†] and Susan Strome[†]

[*]Department of Biological Sciences, Michigan Technological University, Houghton, MI 49931

[†]Department of Molecular, Cell and Developmental Biology, University of California Santa Cruz, Santa Cruz, CA 95064

Interrupting DREAM complex formation

Keywords

DREAM, pocket protein, MuvB, CRISPR/Cas9 genome editing, transcriptional repression

Corresponding author:

Paul D. Goetsch

740 Dow ESE building

1400 Townsend Drive

Houghton, MI 49931

Phone: 906-487-1790

Email: pdgoetsc@mtu.edu

Abstract

The mammalian pocket protein family, which includes the Retinoblastoma protein (pRb) and Rb-like pocket proteins p107 and p130, regulates entry into and exit from the cell cycle by repressing cell cycle gene expression. Although pRb plays a dominant role in mammalian systems, p107 and p130 are the ancestral pocket proteins. The Rb-like pocket proteins interact with the highly conserved 5-subunit MuvB complex and an E2F-DP transcription factor heterodimer, forming the DREAM (for Dp, Rb-like, E2F, and MuvB) complex. DREAM complex assembly on chromatin culminates in repression of target genes mediated by the MuvB subcomplex. Here, we examined how the Rb-like pocket protein contributes to DREAM formation and function by disrupting the interaction between the sole *Caenorhabditis elegans* pocket protein LIN-35 and the MuvB subunit LIN-52 using CRISPR/Cas9 targeted mutagenesis. A triple alanine substitution of LIN-52's LxCxE motif severed LIN-35-MuvB association and caused classical DREAM mutant phenotypes, including synthetic multiple vulvae, high-temperature arrest, and ectopic expression of germline genes in the soma. However, RNA-seq revealed limited upregulation of DREAM target genes when LIN-35-MuvB association was severed, as compared to gene upregulation following LIN-35 loss. Based on chromatin immunoprecipitation, disrupting LIN-35-MuvB association did not affect the chromatin localization of E2F-DP, LIN-35, or MuvB components. In a previous study we showed that in worms lacking LIN-35, E2F-DP and MuvB chromatin occupancy was reduced genome-wide. With LIN-35 present but unable to associate with MuvB, our present study suggests that the E2F-DP-LIN-35 interaction promotes E2F-DP's chromatin localization, which we hypothesize supports MuvB chromatin

occupancy indirectly through DNA. Altogether, this study highlights how the pocket protein's association with MuvB supports DREAM function but is not required for DREAM's chromatin occupancy.

Introduction

Members of the mammalian Retinoblastoma (Rb) protein family, pRb, p107, and p130, collectively called pocket proteins, serve key roles in regulating transcription during the cell cycle (CLASSON AND DYSON 2001; CLASSON AND HARLOW 2002; COBRINIK 2005; BURKHART AND SAGE 2008; DICK AND RUBIN 2013). In mammalian cells, pRb interacts with activating E2F-DP transcription factor heterodimers (in mammals, E2F1/2/3-DP1/2), sequestering E2F-DP and preventing E2F-DP-mediated activation of early cell cycle genes (HELIN *et al.* 1992; LEES *et al.* 1993; LIBAN *et al.* 2016). In contrast, the Rb-like proteins p107 and p130 interact with repressive E2F-DPs (in mammals, E2F4/5-DP1/2) and a highly conserved 5-subunit MuvB subcomplex (in mammals, LIN9, LIN37, LIN52, LIN54, and RBAP48), forming the 8-subunit DREAM transcriptional repressor complex (KORENJAK *et al.* 2004; LEWIS *et al.* 2004; HARRISON *et al.* 2006; LITOVCHICK *et al.* 2007; SCHMIT *et al.* 2007). When associated with the DREAM complex, MuvB mediates transcriptional repression of early and late cell cycle genes (LITOVCHICK *et al.* 2007; GOETSCH *et al.* 2017; MULLER *et al.* 2017). The transcriptional functions of the DREAM complex and pRb overlap, with each being sufficient to establish and maintain cellular quiescence (G_0) if the other is inactive (HURFORD *et al.* 1997; LITOVCHICK *et al.* 2007; MULLER *et al.* 2017). Upon progression into the cell cycle, pRb and the Rb-like pocket proteins are phosphorylated by CDK4/6-cyclin D, releasing their respective interaction partners and triggering activation of cell cycle genes (TEDESCO *et*

93 *al.* 2002; PILKINTON *et al.* 2007; BURKE *et al.* 2010). Thus, the association and
94 dissociation of pocket proteins from their respective transcriptional complexes governs
95 the switch between cell cycle quiescence and cell cycle progression.

96 The Rb-like homologs p130 and p107 are the ancestral pocket proteins and likely
97 the conserved components that mediate cell cycle control among eukaryotes (CAO *et al.*
98 2010; LIBAN *et al.* 2017). In *C. elegans*, LIN-35 is the sole pocket protein, most closely
99 resembling p130/p107 (LU AND HORVITZ 1998). The pocket protein-associated complex
100 MuvB was isolated in *Drosophila melanogaster* (KORENJAK *et al.* 2004; LEWIS *et al.*
101 2004) and *Caenorhabditis elegans* (HARRISON *et al.* 2006) before homologs were
102 identified in mammals (LITOVCHICK *et al.* 2007; PILKINTON *et al.* 2007; SCHMIT *et al.*
103 2007). The *C. elegans* complex, variably called DRM and DREAM, regulates cell cycle
104 genes and requires MuvB to mediate gene repression (BOXEM AND VAN DEN HEUVEL
105 2002; GOETSCH *et al.* 2017). *C. elegans* DREAM also regulates cell-fate specification by
106 antagonizing Ras signaling during vulval development (MYERS AND GREENWALD 2005;
107 CUI *et al.* 2006; HARRISON *et al.* 2006) and by protecting somatic cells from expressing
108 germline genes (WANG *et al.* 2005; PETRELLA *et al.* 2011).

109 Extensive biochemical analyses have demonstrated how the DREAM complex
110 assembles on chromatin (Figure 1A) (LITOVCHICK *et al.* 2007; PILKINTON *et al.* 2007;
111 SCHMIT *et al.* 2007; GUILEY *et al.* 2015; ASTHANA *et al.* 2022). E2F-DP and LIN54, a
112 MuvB component, direct site-specific chromatin localization (ZWICKER *et al.* 1995;
113 SCHMIT *et al.* 2009; MULLER AND ENGELAND 2010; MULLER *et al.* 2012; MARCEAU *et al.*
114 2016). The Rb-like pocket protein serves as a bridge between the 2 DNA-binding
115 DREAM components (GUILEY *et al.* 2015). LIN52 interacts with the pocket protein via an

116 “LxCxE motif” in LIN52. In mammals, the LxCxE motif is instead a suboptimal LxSxExL
117 sequence that is rendered optimal by phosphorylation of a nearby serine residue (S28)
118 (GUILEY *et al.* 2015) (Figure 1B). S28 phosphorylation by DYRK1A kinase induces
119 formation of mammalian DREAM (LITOVCHICK *et al.* 2011). In *C. elegans*, the conserved
120 *lin-52* gene encodes the optimal LxCxE sequence (Figure 1B). *C. elegans* lacks a
121 DYRK1A homolog and its corresponding consensus motif RxSP in LIN-52 (Figure 1B),
122 suggesting that in *C. elegans* a phospho-switch does not induce DREAM formation
123 (LITOVCHICK *et al.* 2011; GUILEY *et al.* 2015). Importantly, the LxCxE binding motif
124 mediates a high-affinity interaction that is employed by the human papillomavirus (HPV)
125 viral oncoprotein E7 to prevent association of LIN52 with the mammalian pocket protein
126 p130 (GUILEY *et al.* 2015).

127 Here, we assessed how the Rb-like pocket protein contributes to DREAM
128 complex formation and function on chromatin. We previously reported that the absence
129 of LIN-35 results in a genome-wide decrease in chromatin occupancy of both E2F-DP
130 and MuvB, illustrating how DRM/DREAM disassembly likely proceeds during cell cycle
131 progression (GOETSCH *et al.* 2017). The model of DREAM complex assembly centers on
132 reintroduction of the pocket protein associations with E2F-DP and MuvB as cells finish
133 the cell cycle (GUILEY *et al.* 2015). To test this model, we used CRISPR/Cas9-mediated
134 genome editing of the *C. elegans* LIN-52 subunit of MuvB to sever the association of
135 LIN-35 with the MuvB subcomplex. Disrupting that association caused phenotypes
136 associated with impairment of DREAM function, including a highly penetrant synthetic
137 multivulval (SynMuv) phenotype (FAY AND YOCHEM 2007), high-temperature larval arrest
138 (PETRELLA *et al.* 2011), and ectopic expression of germline genes in the soma (WANG *et*

139 *al.* 2005; PETRELLA *et al.* 2011). However, our genome-wide transcript analysis revealed
140 that severing the association of LIN-35 and LIN-52 led to upregulation of a relatively
141 small set of DREAM target genes, which displayed a lower magnitude of upregulation
142 than caused by loss of LIN-35. Moreover, chromatin immunoprecipitation (ChIP)
143 revealed that the chromatin association of E2F-DP-LIN-35 and MuvB was not impaired
144 by loss of LIN-35-MuvB association, even in gene promoters of upregulated DREAM
145 target genes. Altogether, our results indicate that loss of the direct association between
146 LIN-35 and MuvB causes limited upregulation of DREAM target genes, likely due to
147 DREAM chromatin occupancy being relatively normal, but even those minimal effects
148 lead to phenotypes consistent with impaired DREAM function in *C. elegans*.

149 **Materials and Methods**

150 **Worm strains**

151 Strains were cultured on Nematode Growth Medium (NGM) agarose plates with *E. coli*
152 OP50 and incubated at 20°C. The following strains were used: Wild type N2 (Bristol),
153 SS1240 *lin-52(bn132(lin-52p::TagRFP-T^SEC^3xFLAG::lin-52 3' UTR)) III / hT2G [bli-*
154 *4(e937) let-?(q782) qIs48] (I:III)*, SS1241 *lin-52(bn133(lin-52p::TagRFP-T::3xFLAG::lin-*
155 *52 3' UTR)) III / hT2G [bli-4(e937) let-?(q782) qIs48] (I:III)*, SS1325 *lin-52(bn138(lin-*
156 *52::GFP^SEC^3xFLAG)) III*, SS1256 *lin-52(bn139(lin-52::GFP::3xFLAG)) III*, SS1273
157 *lin-52(bn150(lin-52[C44A]::GFP::3xFLAG)) III*, SS1276 *lin-52(bn151(lin-*
158 *52[L42A,C44A,E46A]::GFP ::3xFLAG)) III*, SS1350 *lin-52(bn139) III; lin-15A(n767) X,*
159 SS1351 *lin-52(bn150) III; lin-15A(n767) X*, SS1352 *lin-52(bn151) III; lin-15A(n767) X*,
160 SS1406 *lin-8(n2731) II; lin-52(bn139) III,* SS1407 *lin-8(n2731) II; lin-52(bn150) III,*
161 SS1408 *lin-8(n2731) II; lin-52(bn151) III*, PDG29 *lin-52(bn139) III; pgl-1(sam52[pgl-*

162 *1::mTagRFPT::3xFLAG]) IV*, PDG30 *lin-52(bn150) III; pgl-1(sam52) IV*, and PDG31 *lin-*
163 *52(bn151) III*; *pgl-1(sam52) IV.*

164 **CRISPR/Cas9-mediated genome editing**

165 For all genomic edits, 20 nucleotide crDNA targeting sequences were identified
166 using the MIT CRISPR design tool (http://crispr.mit.edu). Single guide RNA sequences
167 were cloned into the PU6::unc119_sgRNA vector (Addgene plasmid #46169) using the
168 overlapping PCR fragment method described in (FRIEDLAND *et al.* 2013) or were cloned
169 into pDD162 (Addgene plasmid #47549) using the Q5 Site Directed Mutagenesis Kit
170 (New England Biolabs), as described in (DICKINSON *et al.* 2013). Homologous repair
171 templates were cloned into pDD282 (Addgene plasmid #66823) or pDD284 (Addgene
172 plasmid #66825) using Glibson Assembly (New England Biolabs) (GIBSON *et al.* 2009),
173 as described in (DICKINSON *et al.* 2015). CRISPR/Cas9 component plasmids were co-
174 injected with marker plasmids (FROKJAER-JENSEN *et al.* 2008) to identify strains with an
175 extra-chromosomal array instead of a mutated endogenous gene. For targeted
176 mutagenesis, *dpy-10(cn64)* sgRNA (pJA58, Addgene plasmid #59933), and *dpy-*
177 *10(cn64)* ssDNA template, *dpy-10(cn64)* guide and ssDNA template were co-injected to
178 select for positive CRISPR activity in injectant progeny, as described in (ARRIBERE *et al.*
179 2014). Additional details are provided in Supplemental Materials and Methods.

180 **Microscopy**

181 L1 and L4 larvae were mounted on a 10% agarose pad and immobilized in a 1-2
182 µL suspension of 0.1 µm polystyrene beads (Polysciences), as described in (KIM *et al.*
183 2013). Fluorescence images of L1 larvae were acquired using a Leica DM4B upright
184 microscope with QImaging QIClick camera. Fluorescence images of L4 larvae were

185 acquired using a Solamere spinning-disk confocal system with μManager software
186 (EDELSTEIN *et al.* 2014). The confocal microscope setup was as follows: Yokogawa
187 CSUX-1 spinning disk scanner, Nikon TE2000-E inverted stand, Hamamatsu ImageEM
188 X2 camera, solid state 405-, 488-, and 561-nm laser lines, 435–485, 500–550, and
189 573–613 fluorescent filters, and Nikon Plan Fluor 40x air objective. Images were
190 processed using Image J (SCHNEIDER *et al.* 2012).

191 ***C. elegans* phenotype scoring**

192 For brood size analyses, L4 individuals were cloned to fresh plates every 24
193 hours and all progeny were counted. For SynMuv phenotype scoring, 3 replicate plates
194 per strain were set up with 5-10 adults that were allowed to lay eggs for 6 hours.
195 Progeny were incubated at 20°C for 3 days, then scored for the presence or absence of
196 pseudovulvae. The percentages of multivulva worms in each replicate population were
197 averaged, and the standard deviation was calculated. For HTA phenotype scoring, L4
198 larvae of each strain were incubated at 24°C or 26°C overnight, then 3 plates per strain
199 were set up with 9-12 adults that were allowed to lay eggs for 4-5 hours. Progeny
200 incubated at 24°C or 26°C were counted 2 days later and scored as arrested larvae
201 (HTA) or adults (not HTA). Results from each plate were combined for each strain.

202 **Immunoblotting and co-immunoprecipitation (co-IP)**

203 For immunoblotting whole worm lysates, 200 adults from each strain were picked
204 into SDS gel-loading buffer (50 mM pH 6.8 Tris-Cl, 2% sodium dodecyl sulfate, 0.1%
205 bromophenol blue, 100 mM β-mercaptoethanol). For co-IP, embryos collected after
206 bleaching gravid worms were aged for 3.5 hours and then frozen in liquid nitrogen, and
207 lysates were prepared as described in (GOETSCH *et al.* 2017). For each IP, 8 mg of

208 protein lysate was mixed with antibody-conjugated Dynabeads (ThermoFisher) and
209 incubated for 2 hours at 4°C. Proteins were separated by SDS/PAGE, and western blot
210 analysis was performed using a 1:1,000-1:5000 dilution of primary antibody and 1:2,000
211 dilution of an appropriate HRP-conjugated secondary antibody. Serial western blot
212 analysis was performed by stripping the blot with buffer containing 0.2M pH 2.2 glycine,
213 0.1% SDS, and 1% Tween-20 between antibody probings. Additional details are
214 provided in Supplemental Materials and Methods.

215 **Chromatin immunoprecipitation (ChIP) and sequential ChIP**

216 Embryos collected after bleaching gravid worms were aged for 3.5 hours and
217 then frozen in liquid nitrogen. Lysates were prepared by grinding, crosslinking for 10
218 minutes in 1% formaldehyde, and sonicating to an average size of 250 base pairs in FA
219 buffer (50 mM HEPES/KOH pH 7.5, 1 mM EDTA, 1% Triton X-100, 0.1% sodium
220 deoxycholate, 150 mM NaCl) using a Bioruptor (Diagenode) on the high setting with 60
221 rounds of 30 seconds on and 1 minute rest. Protein concentrations of lysates were
222 determined using a Qubit fluorometer. ChIP and sequential ChIP experiments were
223 performed as described in (GOETSCH *et al.* 2017) and in Supplemental Materials and
224 Methods. Quantitative PCR was performed using SYBR green reagents on an Applied
225 Biosystems QuantStudio 3 and ViiA 7 Real-Time PCR Systems (ThermoFisher).

226 **Analysis of transcript levels by RT-qPCR and RNA-seq**

227 Embryos collected after bleaching gravid worms were aged for 3.5 hours and
228 then frozen in Trizol for RNA isolation. A total of 1 µg RNA was treated with DNase and
229 reverse transcribed using the High Capacity cDNA Kit (Applied Biosystems). qPCR was
230 performed using SYBR green reagents on an Applied Biosystems QuantStudio 3 Real-

231 Time PCR System (ThermoFisher). The relative quantity of experimental transcripts
232 was calculated with *act-2* as the control gene using the ΔCt method.
233 RNA-seq libraries were prepared using the NEBNext Poly(A) mRNA Magnetic
234 Isolation Module and NEBNext Ultra II Directional RNA Library Prep Kit for Illumina
235 (New England Biolabs). Samples were multiplexed using the NEBNext Multiplex Oligos
236 for Illumina (NEB). Libraries were sequenced on an Illumina HiSeq X system by
237 Novogene Corporation Inc. (Davis, CA) to acquire 150-bp paired-end reads. Sequence
238 reads were trimmed using fastp (CHEN *et al.* 2018) and mapped to transcriptome
239 version WBcel235 using STAR (DOBIN *et al.* 2013). Read counts per transcript were
240 obtained using HTSeq (ANDERS *et al.* 2015) and differentially expressed genes were
241 assessed using DEseq2 (LOVE *et al.* 2014).
242 **Quantification and statistical analysis**
243 For brood size analysis, significance was determined using a Wilcoxon-Mann-
244 Whitney test comparing CRISPR/Cas9-genome edited strains to wild type (N2). For
245 genome-wide differential expression analysis of *lin-52(3A)* versus *lin-52(WT)* late
246 embryos, we used a 1.5-fold change and adjusted p-value less than 0.05 cutoff as
247 calculated by the Benjamini-Hochberg method performed by DEseq2. For expression
248 analysis of *lin-35(n745)* vs N2 L1s, statistical analysis was performed using R using the
249 Quantile normalization and Robust Multichip Average (RMA) algorithm in the affy
250 package of Bioconductor using the a 1.5-fold change and adjusted p-value less than
251 0.05 cutoff (BOLSTAD *et al.* 2003; IRIZARRY *et al.* 2003). For transcript level analysis by
252 RT-qPCR, significance was determined using a student's t-test between *lin-35* versus
253 wild type (N2) or *lin-52(1A) or lin-52(3A)* versus *lin-52(WT).* For ChIP-qPCR

254 experiments assessing individual subunit's occupancy changes between strains,
255 significance was determined using a student's t-test between *lin-35* versus wild type
256 (N2) or *lin-52(3A)* versus *lin-52(WT).*

257 **Data and reagent availability**

258 Requests for information, strains, and reagents should be directed to and will be
259 fulfilled by Paul D. Goetsch (pdgoetsc@mtu.edu). Supplemental material is available at
260 FigShare. Supplemental information includes supplemental Materials and Methods.
261 Figure S1 contains full western blots presented in Figure 2D. Figure S2 contains full
262 western blots presented in Figure 3B. Figure S3 contains additional DREAM target
263 genes tested using qPCR for ChIP and sequential ChIP analyses to complement Figure
264 6. Antibodies used for western blot and ChIP analyses are available in Supplemental
265 Table S1. Primers used for cloning and qPCR are available in Supplemental Table S2.
266 DESeq2 differential gene expression analysis data are available in Supplemental Table
267 S3. RNA-seq expression data used in this study are available from the Gene
268 Expression Omnibus (GEO; http://www.ncbi.nlm.nih.gov/geo) through GEO Series
269 accession number GSE199287. Microarray expression analysis data used in this study
270 are available through GEO Series accession number GSE6547 (KIRIENKO AND FAY
271 2007).

272 **Results**

273 **Targeted mutagenesis to disrupt *C. elegans* DREAM complex formation**

274 Structural studies previously demonstrated that MuvB interacts with the pocket
275 protein via the LIN52 subunit (Figure 1A) (GUILEY *et al.* 2015). Using the self-excising
276 cassette (SEC) method for *C. elegans* CRISPR/Cas9 genome editing (DICKINSON *et al.*

277 2015), we generated a *lin-52(KO)* strain (*lin52(bn133[lin-52p::TagRFP-T::3xFLAG]*) by
278 completely replacing *lin-52* coding sequence with *TagRFP-T* coding sequence (Figure
279 2A). We observed that *lin-52(KO)* rendered worms sterile (Figure 2C), as previously
280 observed in the *lin-52(n3718)* protein null strain (CEOL *et al.* 2006; HARRISON *et al.*
281 2006). This resembles loss of other MuvB components, as loss of LIN-9, LIN-53 (*C.*
282 *elegans* RBAP48), or LIN-54 in protein null strains also renders worms sterile and
283 affects the levels of other MuvB subunits, suggesting that MuvB components require co-
284 expression for assembly/stability of the complex (HARRISON *et al.* 2006). Loss of LIN-37
285 does not cause sterility and does not affect assembly of the rest of MuvB in either *C.*
286 *elegans* or mammalian cells (HARRISON *et al.* 2006; MAGES *et al.* 2017). We next
287 replaced the *TagRFP-T* coding sequence with *lin-52* tagged with a C-terminal *GFP-*
288 *3xFLAG* coding sequence, generating the *lin-52(WT)* strain (*lin-52(bn139[lin-*
289 *52::GFP::3xFLAG]),* Figure 2A). *lin-52(WT)* completely rescued fertility (Figure 2C),
290 indicating that the GFP tag does not impair LIN-52 function.

291 Since LIN-52 is essential for *C. elegans* fertility, we sought to disrupt the LIN-35-
292 LIN-52 interaction without affecting protein integrity. We directed targeted mutagenesis
293 of the LIN-52 LxCxE sequence (Figure 1B) using CRISPR/Cas9-mediated genomic
294 editing. We generated 2 mutants of the LxCxE binding motif in *lin-52(WT)* using the *dpy-*
295 *10* co-CRISPR method of small oligo homology-directed repair (ARRIBERE *et al.* 2014).
296 We generated the *lin-52(1A)* single-alanine mutation strain (*lin-52(bn150[lin-*
297 *52[C44A]::GFP::3xFLAG)*) and the *lin-52(3A)* triple-alanine mutation strain (*lin-*
298 *52(bn151(lin-52[L42A,C44A,E46A]::GFP::3xFLAG)*) (Figure 2B) with the intent to
299 completely disrupt LIN-52's interaction with the *C. elegans* pocket protein LIN-35.

300 Additional silent mutations were included in the oligo repair templates to generate new
301 restriction enzyme cut sites to aid in genotyping (Figure 2B).
302 Full loss of *C. elegans* DREAM activity causes sterility, as observed in protein
303 null mutants of worm E2F-DP (*dpl-1* and *efl-1)* and worm MuvB (*lin-9, lin-52, lin-53, and*
304 *lin-54)* (BEITEL *et al.* 2000; CHI AND REINKE 2006; TABUCHI *et al.* 2011). Since the C-
305 terminally GFP-tagged *lin-52* coding sequence completely rescued *lin-52(KO)* sterility,
306 we were able to test whether *lin-52(1A)* and *lin-52(3A)* impair DREAM function. We
307 observed that neither the 1A nor 3A mutation in the LIN-52 LxCxE sequence caused a
308 significant reduction in brood size (Figure 2C). Using western blot analysis of selected
309 DREAM components from *lin-52(WT)* and mutant lysates, we observed that DREAM
310 component protein levels were unaffected compared to wild type (N2) (Figure 2D,
311 Figure S1). Similarly, using live-image analysis of *lin-52(WT), lin-52(1A),* and *lin-52(3A)*
312 L4 larvae, we observed that LIN-52 level and localization appeared normal in mutants
313 (Figure 2A). Together, these results demonstrate that mutation of the LIN-52 LxCxE
314 sequence does not cause a *lin-52* null phenotype and does not alter the levels and
315 tissue distribution of MuvB components.

316 **The 3A substitution in the LIN-52 LxCxE sequence blocks DREAM assembly**

317 To test whether our CRISPR/Cas9-generated 1A and 3A substitutions disrupt the
318 LIN-35-MuvB association, we performed co-immunoprecipitations (co-IPs) from protein
319 extracts prepared from *lin-52(WT)*, *lin-52(1A)*, and *lin-52(3A)* late embryos. We pulled
320 down LIN-35 and tested for LIN-52 association using the GFP epitope, and we pulled
321 down LIN-52 using either the GFP or FLAG epitope and tested for LIN-35 association
322 (Figure 3, Figure S2). In both co-IP experiments, we observed that LIN-52 association

323 with LIN-35 was lost in *lin-52(3A)* extracts but not in *lin-52(1A)* extracts. In 1A extracts,
324 we observed a weaker association between LIN-52 and LIN-35 when pulling down with
325 an anti-FLAG antibody, but the effect was not replicated with the anti-GFP antibody.
326 The inconsistent results suggest that the 1A substitution weakens but does not
327 eliminate the LIN-52-LIN-35 interaction. Altogether, these results demonstrate that a 3A
328 substitution in the LxCxE sequence is required to sever the protein-protein association
329 between LIN-52 and LIN-35 in *C. elegans*.

330 **Blocking DREAM complex formation causes classic DREAM loss-of-function**
331 **phenotypes**

332 DREAM loss-of-function mutations when paired with SynMuv A gene mutations
333 cause a synthetic multivulval (SynMuv) phenotype (FAY AND YOCHEM 2007), high-
334 temperature larval arrest (PETRELLA *et al.* 2011), and ectopic expression of germline
335 genes in the soma (WANG *et al.* 2005; PETRELLA *et al.* 2011). We reasoned that if
336 DREAM function was affected by severing the LIN-52-LIN-35 association, then we
337 should observe each of the 3 phenotypes above. When paired with SynMuv A allele *lin-*
338 *8(n2731)* (HARRISON *et al.* 2007) or *lin-15A(n767)* (HUANG *et al.* 1994), *lin-52(3A)*
339 resulted in a SynMuv phenotype; *lin-52(WT)* and *lin-52(1A)* did not have this effect
340 (Figure 4A). When worms were grown at high temperature (26°C), *lin-35(3A)* displayed
341 larval arrest; *lin-52(WT)* and *lin-52(1A)* did not cause larval arrest (Figure 4B). When
342 RT-qPCR was used to examine ectopic expression of the germline genes *pgl-1, pgl-3,*
343 and *glh-1*, *lin-52(3A)* caused upregulation of all 3 genes; *lin-52(1A)* caused upregulaton
344 of *pgl-1* and *pgl-3* but not *glh-1* (Figure 4C). To examine ectopic expression by another
345 method, we crossed a germline-specific *pgl-1::rfp* reporter (MARNIK *et al.* 2019) into our

346 *lin-52* mutant strains. We observed ectopic expression of *pgl-1::rfp* in *lin-52(1A)* and *lin-*
347 *52(3A)* in the intestinal cells of larvae (Figure 4D, E), as expected (PETRELLA *et al.*
348 2011). These phenotypes along with our co-immunoprecipitation findings demonstrate
349 that the 3A substitution has a greater impact on DREAM assembly and function than the
350 1A substitution.

351 **Severing the LIN-35-MuvB connection has a minimal effect on repression of**
352 **DREAM target genes**

353 To investigate whether blocking DREAM assembly affects transcriptional
354 repression of DREAM target genes, we performed whole-genome RNA-sequencing
355 (RNA-seq) in *lin-52(WT)* and *lin-52(3A)* late embryos and compared our data to
356 microarray-based expression data from wild-type and *lin-35(n745)* null mutant L1 larvae
357 (KIRIENKO AND FAY 2007). Our RNA-seq analysis detected 16,855 transcripts (>10
358 counts across samples), as compared to 16,810 transcripts tested in the microarray
359 experiment (Supplemental Table S3, S4). A total of 13,721 transcripts are shared
360 between the two experiments, including 1,370 of the 1,515 genes previously reported to
361 have DREAM bound to their promoters, which we categorize as DREAM targets
362 (GOETSCH *et al.* 2017). In *lin-35(n745)* versus wild-type (N2) L1 larvae, 798 genes (246
363 DREAM targets) were upregulated and 540 genes (31 DREAM targets) were
364 downregulated (Figure 5A). In contrast, in *lin-52(3A)* versus *lin-52(WT)* late embryos,
365 102 genes (32 DREAM targets) were upregulated and 9 genes (0 DREAM targets) were
366 downregulated (Figure 5B). Altogether, our transcript analyses reveal that the 3A
367 substitution has a minimal effect on DREAM target regulation, with only ~2% (32/1370)

368 of DREAM targets upregulated in *lin-52(3A)* late embryos compared to ~18%
369 (246/1370) of DREAM targets upregulated in *lin-35(n745)* L1s.
370 To directly compare at one developmental stage the effect on transcription of
371 loss of LIN-35 versus severing the LIN-35-MuvB association, we assessed transcript
372 levels of a subset of DREAM target genes in *N2, lin-35(n745), lin-52(WT)*, *lin-52(1A)*,
373 and *lin-52(3A)* late embryos using RT-qPCR analysis (Figure 5C,D). We tested 6
374 DREAM target genes that were upregulated (Figure 5C) and 6 DREAM target genes
375 that were not upregulated in *lin-52(3A)* late embryos (Figure 5D), as identified from our
376 RNA-seq analysis. For the 6 DREAM target genes that were upregulated in our RNA-
377 seq analysis (*C09G5.7, set-21, polh-1, ZK795.2, rnf-1,* and *Y47G6A.3),* we consistently
378 observed 1) modest but significant upregulation in *lin-52(3A)* versus *lin-52(WT) and* 2) a
379 greater increase in transcript levels in *lin-35* versus N2 than in *lin-52(3A)* versus *lin-*
380 *52(WT)* (Figure 5C). Consistent with our phenotype analysis, we observed that *lin-*
381 *52(1A)* had a minimal effect on DREAM target gene levels (Figure 5C). For the 6
382 DREAM target genes that were not upregulated in our RNA-seq analysis (*cdk-1, air-1,*
383 *mis-12, rad-51, kbp-3,* and *polk-1*), we did not observe an increase in transcript levels in
384 *lin-52(3A)* or *lin-52(1A)* compared to *lin-52(WT)* (Figure 5D). Most (4 of 6) of these
385 genes were significantly upregulated in *lin-35* versus N2 late embryos. Altogether, our
386 RNA-seq and RT-qPCR analyses demonstrate that blocking DREAM assembly has a
387 limited impact on DREAM target gene repression in late embryos, in terms of both
388 number of genes upregulated and the amplitude of upregulation, as compared to
389 complete loss of LIN-35.

390 **E2F-DP-LIN-35 and MuvB subcomplexes independently co-occupy chromatin**
391 **sites**

392 In the absence of LIN-35, E2F-DP and MuvB do not associate with one another
393 and their chromatin occupancy is reduced genome-wide (GOETSCH *et al.* 2017). In our
394 *lin-52(3A)* worm strain, LIN-35 is present, but its association with MuvB is severed. We
395 tested the impact of this severing on the chromatin localization of DREAM components
396 using chromatin immunoprecipitation (ChIP). We chose 2 DREAM target genes that in
397 our RNA-seq analysis were upregulated in *lin-52(3A)* (*set-21* and *polh-1*; Figure 6A),
398 and 2 DREAM target genes that were not upregulated in *lin-52(3A)* (*air-1* and *mis-12*;
399 Figure 6B). We performed ChIP-qPCR of DPL-1 and LIN-37 in *lin-35* null compared to
400 N2 embryos, and DPL-1, LIN-35, LIN-37, and LIN-52 via its GFP tag in *lin-52(3A)*
401 compared to *lin-52(WT)* embryos. IgG was used as a negative control for both ChIP
402 analyses. We observed that all tested DREAM components remained similarly enriched
403 at the 4 selected promoters in *lin-52(3A)* as compared to *lin-52(WT)* (Figure 6A,B). In
404 contrast, chromatin occupancy of both DPL-1 and LIN-37 were significantly reduced in 3
405 of the 4 selected promoters in *lin-35(n745)* as compared to N2. An additional 8 DREAM
406 target gene promoters were tested and showed similar DREAM chromatin occupancy
407 profiles (Figure S3A,B). We did observe that LIN-37 and LIN-52 chromatin occupancy
408 was reduced at some DREAM target gene promoters, but the observed decrease did
409 not correspond to whether the target gene is misregulated (Figure S3A,B). Notably, the
410 key difference between *lin-35(n745)* and *lin-52(3A)* is the status of the pocket protein.
411 Since DPL-1 and LIN-35 occupancy is not compromised by severing the LIN-52-LIN-35
412 association in *lin-52(3A)* while DPL-1 occupancy is compromised by loss of LIN-35, our

413 results suggest that the chromatin association of the repressive E2F-DP transcription
414 factor heterodimer is stabilized by its interaction with LIN-35.

415 We tested whether MuvB and E2F-DP-LIN-35 co-occupy DREAM target regions
416 by performing sequential ChIP analysis. We first ChIPed LIN-52 via its FLAG tag and
417 then ChIPed LIN-35. We observed no significant difference in LIN-52 and LIN-35 co-
418 occupancy in *lin-52(3A)* extracts versus *lin-52(WT)* extracts at 8 DREAM target gene
419 promoters, as determined by a student's t-test (Figure 6C, S3C). Altogether, our results
420 indicate that, although the interaction of LIN-35 and MuvB is disrupted, DREAM
421 components can nevertheless co-localize at target promoters through their respective
422 protein-DNA interactions.

423 **Discussion**

424 We previously postulated that DREAM assembly, initiated by DYRK1A
425 phosphorylation of LIN52 in mammalian cells (LITOVCHICK *et al.* 2011; GUILEY *et al.*
426 2015), stabilizes MuvB-mediated repression of DREAM target genes (GOETSCH *et al.*
427 2017). Using CRISPR/Cas9-mediated targeted mutagenesis, we generated a mutant *C.*
428 *elegans* strain in which LIN-52 was rendered incapable of interacting with LIN-35, the
429 sole *C. elegans* Rb-like pocket protein. We expected that, similar to loss of LIN-35
430 (GOETSCH *et al.* 2017), MuvB chromatin occupancy would be destabilized and its
431 repressive function would be impaired. Instead, we observed that chromatin occupancy
432 was not destabilized at the genes tested and that relatively few genes were
433 upregulated. We observed that ~2% of all DREAM target genes were de-repressed,
434 indicating that for those genes MuvB chromatin occupancy alone is not sufficient for
435 target gene repression. However, interrupting LIN-35-MuvB association did cause

436 classic DREAM mutant phenotypes, including SynMuv, high temperature arrest, and
437 ectopic expression of germline genes in the soma, consistent with impaired DREAM
438 function. Altogether, we conclude that the LIN-35-MuvB association is not required to
439 assemble DREAM at target sites but is necessary for full activity of the complex.

440 Our findings highlight that even minimal perturbation of DREAM-mediated
441 transcriptional repression of target genes causes observable phenotypic consequences
442 in *C. elegans*. Complete knockout of DREAM activity causes sterility, as demonstrated
443 by our newly generated *lin-52* null mutant and null mutants of other DREAM
444 components (HARRISON *et al.* 2006). In contrast, although our RNA-seq analysis
445 revealed that ~2% of DREAM target genes were upregulated in the *lin-52(3A)* mutant,
446 that mutant caused highly penetrant SynMuv phenotypes with no corresponding effect
447 on fertility. Thus, phenotype analysis provides a sensitive readout of DREAM function.

448 How the limited upregulation of some DREAM target genes in *lin-52(3A)* mutant
449 embryos causes the observed phenotypes remains unknown. The SynMuv phenotype
450 is caused by ectopic activation of LIN-3/EGF in the hyp7 hypodermal syncytium, which
451 requires synthetic impairment of redundant regulatory pathways established by SynMuv
452 A and SynMuv B class genes (CUI *et al.* 2006). Although there is some evidence that
453 SynMuv A class proteins directly target *lin-3*'s promoter (SAFFER *et al.* 2011), DREAM
454 does not appear to regulate *lin-3* directly (GOETSCH *et al.* 2017). Similarly, we suspect
455 that DREAM antagonism of high-temperature arrest and ectopic expression of germline
456 genes in the soma is also indirect (PETRELLA *et al.* 2011; GOETSCH *et al.* 2017;
457 RECHTSTEINER *et al.* 2019). Instead, we speculate that SynMuv B class proteins
458 including DREAM regulate chromatin compaction in somatic cells during development

459 (COSTELLO AND PETRELLA 2019). Thus, even minimal perturbation of DREAM complex
460 activity may delay embryonic chromatin compaction, providing a window for alternative
461 regulatory pathways to trigger the developmental defects detected at later larval stages.
462 Our analysis provides important insight into how assembly of the mammalian
463 DREAM complex maintains repression of cell cycle genes and suggests that the pocket
464 protein's primary function is to protect MuvB's function as a transcriptional repressor.
465 DREAM assembly is triggered by DYRK1A phosphorylation of LIN52, initiating MuvB
466 association with p107/p130 (LITOVCHICK *et al.* 2011; GUILEY *et al.* 2015). Mammalian
467 MuvB's function switches from transcriptional repression in the DREAM complex during
468 quiescence to transcriptional activation after associating with the B-Myb transcription
469 factor and forming the Myb-MuvB (MMB) complex late in the cell cycle (LEWIS *et al.*
470 2004; OSTERLOH *et al.* 2007; SCHMIT *et al.* 2007; KNIGHT *et al.* 2009; SADASIVAM *et al.*
471 2012). DYRK1A-mediated LIN52 phosphorylation also inhibits MuvB association with B-
472 Myb (LITOVCHICK *et al.* 2011), even though the 2 interaction interfaces do not physically
473 overlap (GUILEY *et al.* 2018). In *Drosophila,* Lin-52 protein is required for MMB to
474 oppose repressive DREAM functions (LEWIS *et al.* 2012), suggesting that Lin-52's
475 interaction with the pocket protein or B-Myb dictates MuvB's transcriptional function
476 (GUILEY *et al.* 2018). Our data demonstrate that in worms MuvB localizes to chromatin
477 sites and represses gene targets without direct association with the pocket protein.
478 These findings suggest that the pocket protein's association with LIN-52 serves a
479 different purpose than just to direct assembly of DREAM. We propose that the pocket
480 protein's association with LIN-52 instead primarily functions to oppose B-Myb
481 association with MuvB, preventing MuvB from converting to its transcriptionally active

482 role. Since no B-Myb homolog exists in *C. elegans* (VORSTER *et al.* 2020), loss of direct
483 LIN-35-MuvB association had little effect on target gene repression. We predict that a
484 similar 3A mutation in LIN-52 in *Drosophila* or mammalian cells would cause
485 significantly more upregulation of DREAM target genes.

486 The switch between MuvB-associated cell cycle gene repression and activation
487 is hijacked in cancer cells. All 3 mammalian pocket proteins are inactivated by the E7
488 viral oncoprotein present in high-risk human papillovirus (HPV) (ZHANG *et al.* 2006; HUH
489 *et al.* 2007). E7 interacts with the mammalian pocket proteins through its high-affinity
490 LxCxE binding motif, disrupting MuvB association with the pocket protein in DREAM
491 (GUILEY *et al.* 2015). HPV E7 concurrently coaxes MuvB into its transcriptional activator
492 function by stimulating MMB assembly (PANG *et al.* 2014). However, cancer cells resist
493 cytotoxic chemotherapy by temporarily exiting the cell cycle (BOICHUK *et al.* 2013),
494 suggesting that MuvB's capacity for transcriptional repression is retained. Based on our
495 findings that MuvB does not require direct association with the pocket protein to repress
496 target genes, MuvB's function in cancer cells requires closer scrutiny.

497 We previously observed that E2F-DP and MuvB chromatin association is
498 severely affected by loss of LIN-35 (GOETSCH *et al.* 2017). By severing LIN-35-MuvB
499 association, the present study suggests a new model for DREAM complex formation
500 where LIN-35 directly stabilizes E2F-DP chromatin occupancy. We also observed that
501 MuvB chromatin occupancy is not disrupted even though MuvB no longer associates
502 directly with E2F-DP-LIN-35. Importantly, *in vitro* analysis of the DNA-binding
503 characteristics of heterodimeric mammalian E2F-DP identified a distinct induction of
504 DNA bending, especially in the case of the homologues of *C. elegans* EFL-1-DPL-1

505 (E2F4-DP1/2) (TAO *et al.* 1997). We propose that DNA-associated E2F-DP
506 heterodimers promote MuvB co-occupancy through a DNA bending-dependent
507 mechanism. Together, our results suggest a model in which the LIN-35 pocket protein
508 promotes E2F-DP chromatin occupancy, which in turn promotes MuvB chromatin
509 occupancy.

510 Our results support an exciting model for how local E2F-DP-mediated alterations
511 to DNA shape enhanced by their interaction with a pocket protein promote MuvB co-
512 occupancy. Even with evolutionary divergence from the ancestral pocket protein, this
513 model may also apply to pRb function. Many histone deacetylases and chromatin
514 remodeling complexes associate with pRb through the LxCxE binding cleft, although
515 many of these associations have only limited support thus far from
516 structural/biochemical interaction studies (DYSON 2016). Variation in pRb
517 monophosphorylation events that can alter pRb structure and recognition of binding
518 partners offers one explanation for how pRb can potentially interact with >300 individual
519 protein partners (RUBIN 2013; NARASIMHA *et al.* 2014). Our data provide an alternative,
520 but not exclusive, possibility, namely that direct and stable pRb association with these
521 myriad protein partners may be unnecessary. Perhaps pRb association with a few
522 partners such as E2F-DPs promotes localization of multi-protein complexes to genomic
523 sites. Additional dissection of DREAM and pRb structure and function will shed light on
524 how the pocket proteins mediate their essential cellular roles.

525 **Acknowledgments**

526 We thank Seth Rubin and members of the Rubin and Strome labs for helpful
527 discussions. Some strains were provided by the Caenorhabditis Genetics Center, which

is funded by the NIH Office of Research Infrastructure Programs (P40 OD010440). This work was supported by National Institutes of Health R01 grant GM34069 to S.S., American Cancer Society Postdoctoral Fellowship PF-16-106-01-DDC to P.D.G., and National Institutes of Health R15 grant GM137145 to P.D.G.

Figure 1

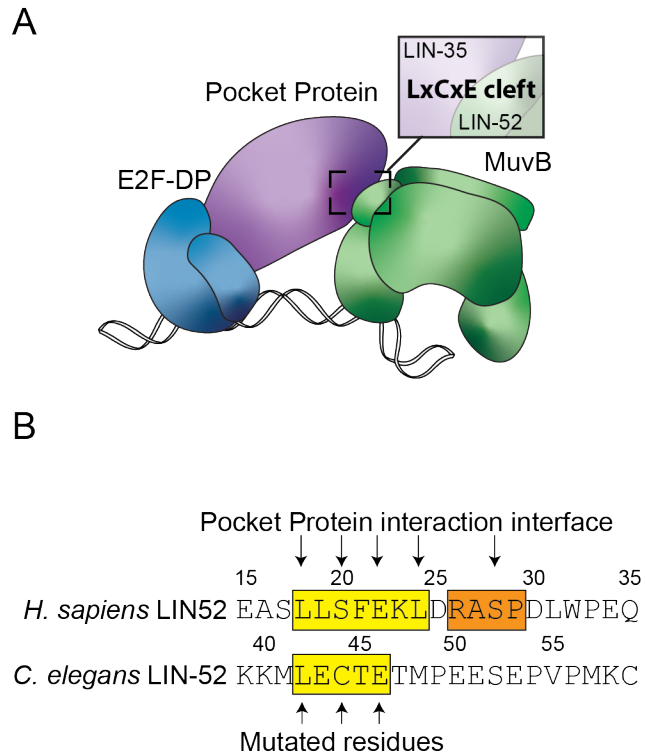

Figure 1 LIN-35 and MuvB associate via the LxCxE motif of LIN-52. (A) Model of the *C. elegans* DREAM complex bound to DNA: E2F-DP (blue), the pocket protein LIN-35 (purple), and the 5-subunit MuvB subcomplex (green). The highlighted region shows the target region for this study: an LxCxE binding motif in the MuvB subunit LIN-52 that interacts directly with the LIN-35 pocket protein. (B) Alignment of *H. sapiens* LIN52 and *C. elegans* LIN-52 sequences. The human LxSxExL and worm LxCxE sequences are highlighted in yellow, and the human DYRK1A consensus phosphorylation sequence is highlighted in orange. Arrows indicate residues involved in the interaction with the pocket protein and amino acid residues converted to alanine in this study.

573 **Figure 2**

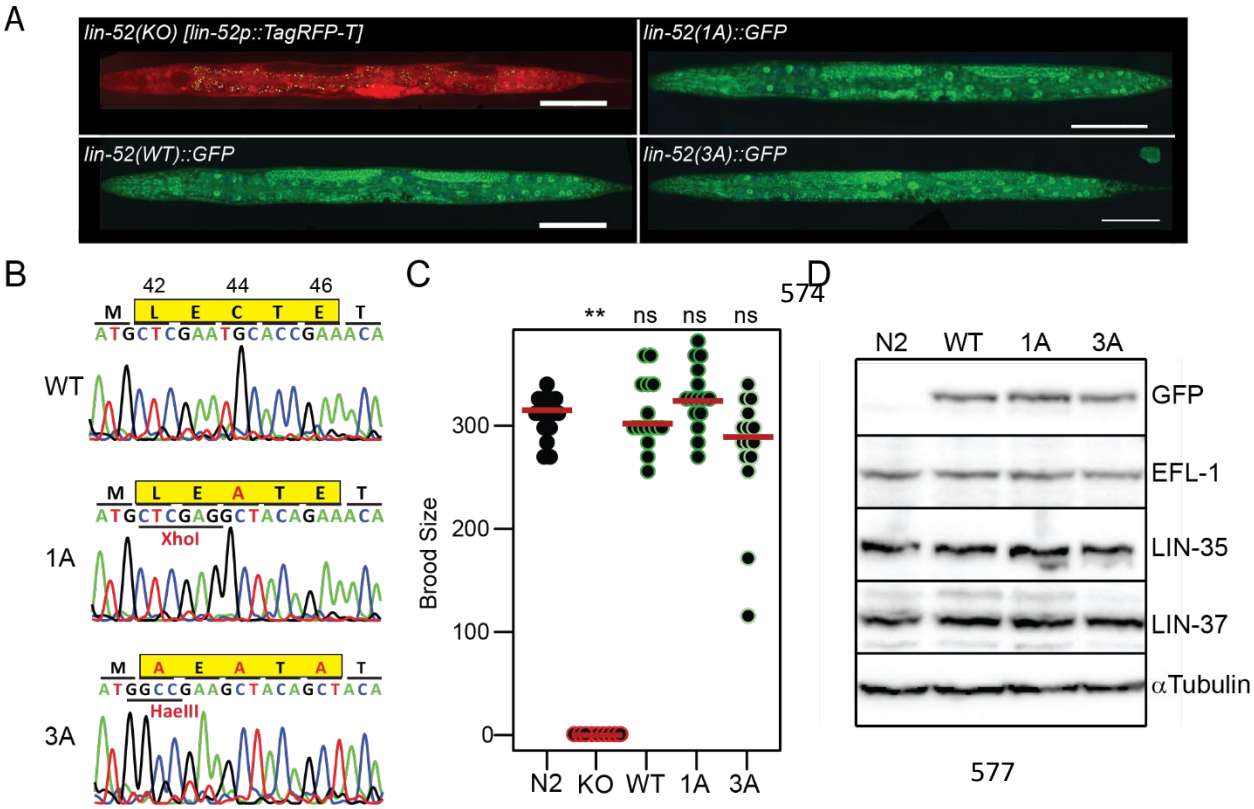

578

579 **Figure 2** Targeted mutagenesis to disrupt DREAM complex formation. (A) Live worm
580 fluorescence images of *lin-52(KO), lin-52(WT*), *lin-52(1A),* and *lin-52(3A)* L4 larvae.
581 Composites were artificially straightened. Scale bars, 100μM. (B) Sanger sequencing of
582 the *lin-52* LxCxE coding region (highlighted in yellow) in *lin-52(WT), lin-52(1A*), and *lin-*
583 *52(3A*). (C) Swarm plots of the brood sizes of wild-type (N2) worms and *lin-52(KO)*, *lin-*
584 *52(WT)*, *lin-52(1A)*, and *lin-52(3A)* transgenic worms. Significance (** p-value < 0.01)
585 was determined by a Wilcoxon-Mann-Whitney test comparing the indicated strains to
586 wild type (N2). (D) Western blot analysis of DREAM subunits LIN-52 (via GFP tag),
587 EFL-1, LIN-35, and LIN-37 using lysates from wild-type (N2) worms and *lin-52(WT), lin-*
588 *52(1A),* and *lin-52(3A)* transgenic worms separated by SDS PAGE. Antibodies used are

589 indicated on the right. Alpha-tubulin was used as a loading control. Full blots are shown
590 in Figure S1.
591
592
593
594
595
596
597
598
599
600
601
602
603
604
605
606
607
608
609
610
611

612 **Figure 3**

613

614

615

616

617

618

619

620

621

622

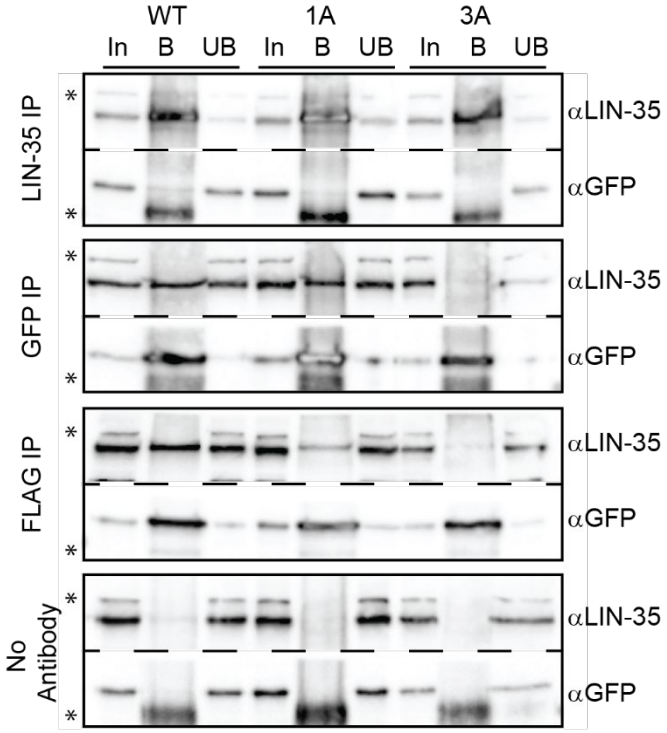

623

624 **Figure 3** *lin-52* LxCxE binding motif mutants block DREAM formation. Late embryo

625 extracts from *lin-52(WT)*, *lin-52(1A)*, and *lin-52(3A)* (each tagged with GFP and FLAG)

626 were immunoprecipitated with anti-LIN-35, anti-GFP, and anti-FLAG antibodies, with no

627 antibody serving as a negative control. Proteins bound (B) and unbound (UB) were

628 separated by SDS PAGE, and western blot analysis was performed using the

629 antibodies indicated on the right. 5% of Input (In) is shown on the left. Asterisks indicate

630 non-specific bands. Full blots are shown in Figure S2.

631

632

633

634

635 **Figure 4**

A

% SynMuv±s.d. (n)

	lin-8(n2731)	*lin-15A(n767)*
WT	0±0 (382)	0±0 (505)
1A	0±0 (211)	0±0 (422)
3A	99.3±0.6 (301)	96.5±0.2 (375)

B

% HTA (n)

	24°C	26°C
WT	0.0 (300)	0.4 (495)
1A	0.0 (322)	0.6 (330)
3A	0.0 (352)	96.8 (501)

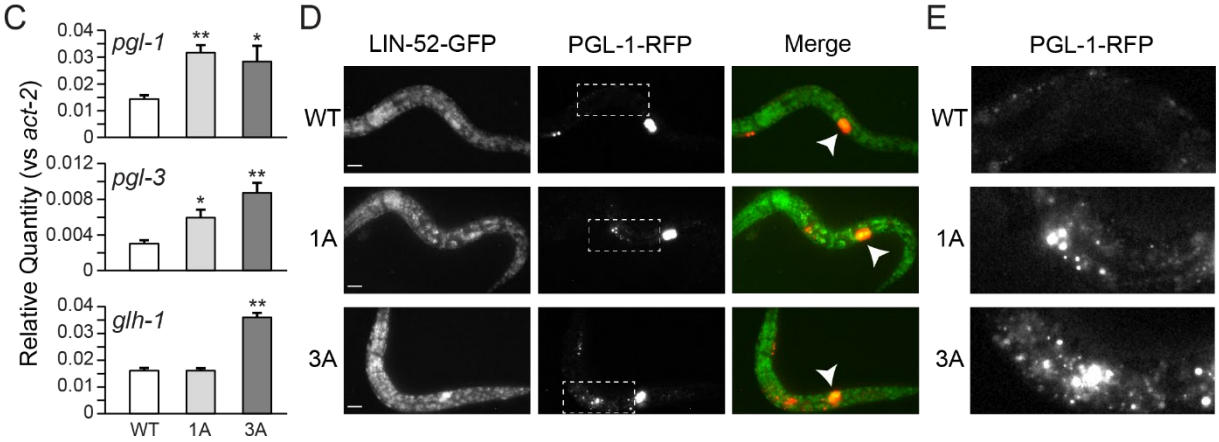

636

637 **Figure 4** Mutagenesis of the *lin-52* LxCxE binding motif causes SynMuv B phenotypes.
638 (A) Table indicating the percentage Synthetic Multivulval (SynMuv) worms when *lin-*
639 *52(WT), lin-52(1A)*, and *lin-52(3A)* were combined with SynMuv A mutant alleles *lin-*
640 *8(n2731)* or *lin-15A(n767)* with standard deviation indicated. The population size (n*)* is
641 indicated in parentheses. (B) Table indicating the percentage of High Temperature
642 Arrest (HTA) observed in *lin-52(WT), lin-52(1A), and lin-52(3A)* incubated at 24°C and
643 26°C. The population size (n) is indicated in parentheses. (C) RT-qPCR analysis
644 comparing transcript levels of 3 germline genes (*pgl-1, pgl-3,* and *glh-1*) in *lin-52(WT)*
645 (white), *lin-52(1A)* (light grey), and *lin-52(3A)* (dark grey) late embryos. Expression
646 values from 6 biological replicates were averaged and are presented as the relative
647 quantity compared to *act-2.* Error bars indicate standard error of the mean, and
648 significance was determined by a student's t-test between transcript levels in mutant

649 (3A or 1A) versus WT (* p-value < 0.05, ** p-value < 0.01). (D,E) Live worm
650 fluorescence images of *lin-52(WT*), *lin-52(1A),* and *lin-52(3A)* L1 larvae containing a
651 PGL-1::RFP reporter gene. White arrowheads indicate the primordial germ cells Z2 and
652 Z3. Scale bars, 10 μm. The white boxes in (D) indicate regions of ectopic expression of
653 PGL-1::RFP in the intestine of *lin-52(1A)* and *lin-52(3A)* shown in (E).
654
655
656
657
658
659
660
661
662
663
664
665
666
667
668
669
670
671

672 **Figure 5**

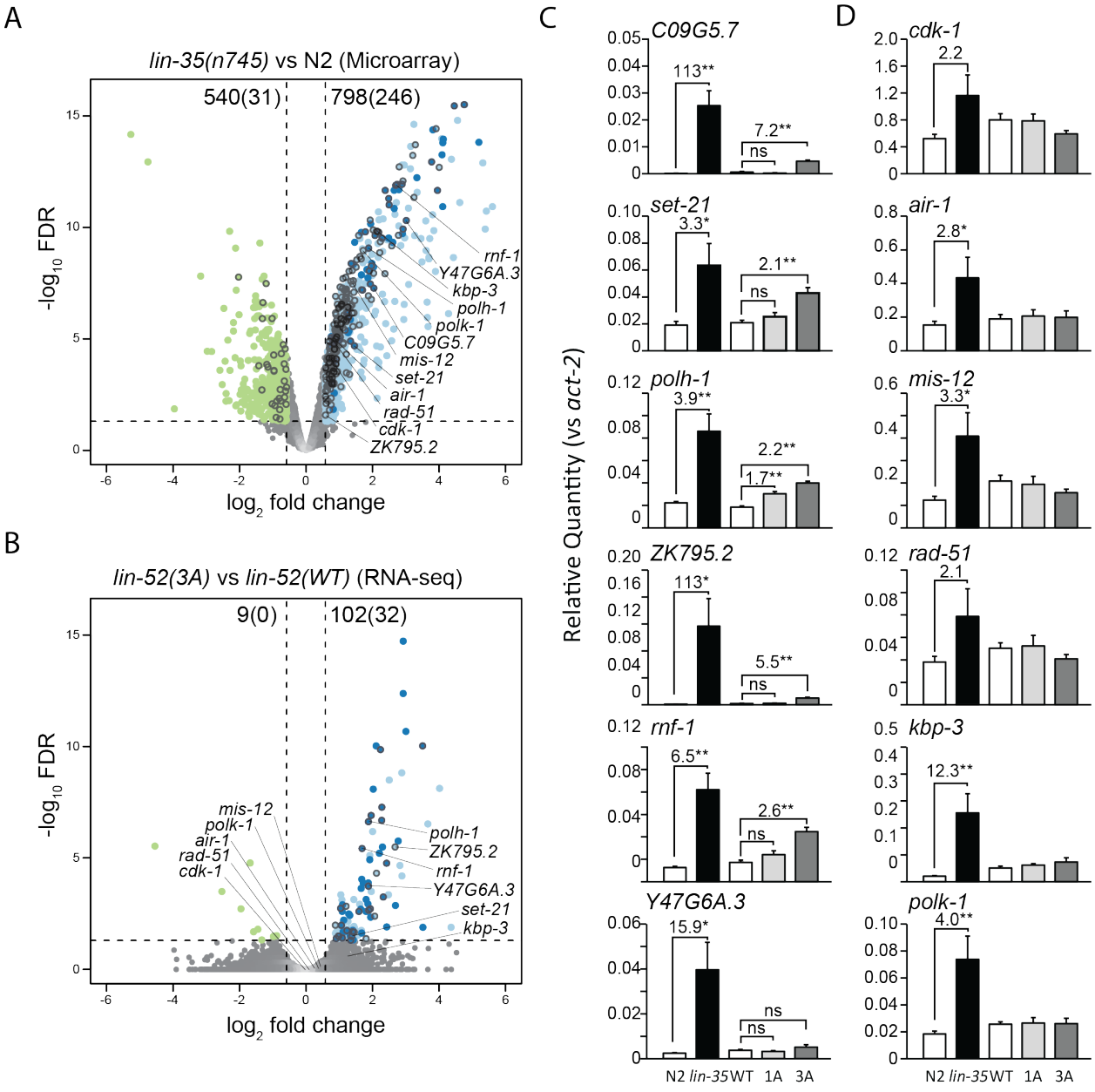

673

674 **Figure 5** Disruption of DREAM formation leads to upregulation of a small subset of

675 target genes. (A,B) Volcano plots of log2 fold change in transcript levels versus log10

676 False Discovery Rate (FDR) of 13,721 genes shared between (A) *lin-35(n745)* versus

677 N2 L1 microarray expression analysis reported in (KIRIENKO AND FAY 2007) and (B) *lin-*

678 *52(3A)* versus *lin-52(WT)* late embryo RNA-seq. Genes downregulated (green) or

679 upregulated (blue) are highlighted, with dark blue indicating upregulated genes
680 observed in both *lin-35* and *lin-52(3A)* data sets. Black circle outlines indicate DREAM
681 target genes, as reported in (GOETSCH *et al.* 2017). The number of genes differentially
682 expressed in each analysis are indicated at the top of each plot, with the number of
683 DREAM target genes differentially expressed indicated in parentheses. Dashed lines
684 indicate the significance cut-off of q = 0.05 (horizontal lines) and a 1.5-fold change in
685 transcript level (vertical lines). Genes selected for RT-qPCR analysis are labeled. (C,D)
686 RT-qPCR analysis comparing transcript levels of 6 DREAM target genes that were
687 upregulated in RNA-seq (C) and 6 DREAM target genes that were not upregulated in
688 RNA-seq (D). Transcript levels in late embryos are from wild type N2 (white), *lin-35*
689 (black), *lin-52(WT)* (white), *lin-52(1A)* (light grey), and *lin-52(3A)* (dark grey). Expression
690 values from 6 biological replicates were averaged and are presented as the relative
691 quantity compared to *act-2.* Error bars indicate standard error of the mean, fold change
692 values greater than 1.5-fold are provided, and significance was determined by a
693 student's t-test between transcript levels in mutant (3A or 1A) versus WT or *lin-35*
694 versus N2 (* p-value < 0.05, ** p-value < 0.01).
695
696
697
698
699
700
701

Figure 6

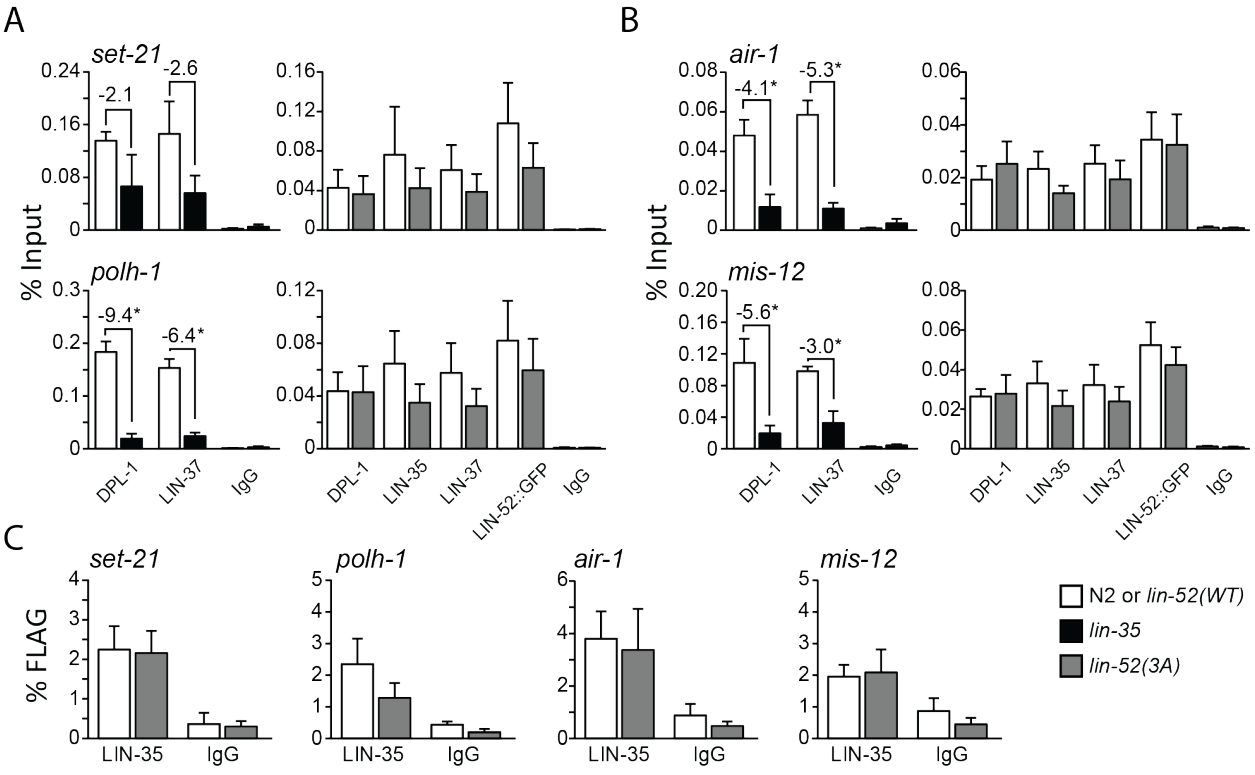

Figure 6 Analysis of chromatin localization of DREAM subunits at target genes. (A,B) ChIP-qPCR of DREAM subunits DPL-1 and LIN-37 in N2 (white) versus *lin-35* (black) and DPL-1, LIN-35, LIN-37, and LIN-52 (via GFP tag) in *lin-52(WT*) (white) versus *lin-52(3A*) (dark grey) late embryo extracts at 2 DREAM target genes that were upregulated in RNA-seq (A) and 2 DREAM target genes that were not upregulated in RNA-seq (B). IgG was used as a negative control. Signals are presented as percentage of Input DNA, with negative fold-change values greater than 2-fold noted. Error bars indicate standard error of the mean. Significance was determined by a student's t-test between subunit ChIP values in mutant (*lin-35* or *lin-52*(*3A)*) versus wild-type control (N2 or *lin-52(WT))* (* p-value < 0.05). (C) Sequential ChIP-qPCR of LIN-52 (via FLAG tag) followed by LIN-35 or IgG from *lin-52(WT*) (white) and *lin-52(3A*) (dark grey) late embryo extracts at 4 DREAM target genes. Signals are presented as percentage of

716 FLAG IP DNA. Error bars indicate standard error of the mean. Additional data are
717 shown in Figure S3.
718
719
720
721
722
723
724
725
726
727
728
729
730
731
732
733
734
735
736
737
738

739 **References**

740 Anders, S., P. T. Pyl and W. Huber, 2015 HTSeq--a Python framework to work with high-
741 throughput sequencing data. Bioinformatics 31**:** 166-169.

742 Arribere, J. A., R. T. Bell, B. X. Fu, K. L. Artiles, P. S. Hartman *et al.*, 2014 Efficient marker-
743 free recovery of custom genetic modifications with CRISPR/Cas9 in
744 Caenorhabditis elegans. Genetics 198**:** 837-846.

745 Asthana, A., P. Ramanan, A. Hirschi, K. Z. Guiley, T. U. Wijeratne *et al.*, 2022 The MuvB
746 complex binds and stabilizes nucleosomes downstream of the transcription start
747 site of cell-cycle dependent genes. Nat Commun 13**:** 526.

748 Beitel, G. J., E. J. Lambie and H. R. Horvitz, 2000 The C. elegans gene lin-9,which acts
749 in an Rb-related pathway, is required for gonadal sheath cell development and
750 encodes a novel protein. Gene 254**:** 253-263.

751 Boichuk, S., J. A. Parry, K. R. Makielski, L. Litovchick, J. L. Baron *et al.*, 2013 The DREAM
752 complex mediates GIST cell quiescence and is a novel therapeutic target to
753 enhance imatinib-induced apoptosis. Cancer Res 73**:** 5120-5129.

754 Bolstad, B. M., R. A. Irizarry, M. Astrand and T. P. Speed, 2003 A comparison of
755 normalization methods for high density oligonucleotide array data based on
756 variance and bias. Bioinformatics 19**:** 185-193.

757 Boxem, M., and S. van den Heuvel, 2002 C. elegans class B synthetic multivulva genes
758 act in G(1) regulation. Curr Biol 12**:** 906-911.

759 Burke, J. R., A. J. Deshong, J. G. Pelton and S. M. Rubin, 2010 Phosphorylation-induced
760 conformational changes in the retinoblastoma protein inhibit E2F transactivation
761 domain binding. J Biol Chem 285**:** 16286-16293.

762 Burkhart, D. L., and J. Sage, 2008 Cellular mechanisms of tumour suppression by the
763 retinoblastoma gene. Nat Rev Cancer 8**:** 671-682.
764 Cao, L., B. Peng, L. Yao, X. Zhang, K. Sun *et al.*, 2010 The ancient function of RB-E2F
765 pathway: insights from its evolutionary history. Biol Direct 5**:** 55.
766 Ceol, C. J., F. Stegmeier, M. M. Harrison and H. R. Horvitz, 2006 Identification and
767 classification of genes that act antagonistically to let-60 Ras signaling in
768 Caenorhabditis elegans vulval development. Genetics 173**:** 709-726.
769 Chen, S., Y. Zhou, Y. Chen and J. Gu, 2018 fastp: an ultra-fast all-in-one FASTQ
770 preprocessor. Bioinformatics 34**:** i884-i890.
771 Chi, W., and V. Reinke, 2006 Promotion of oogenesis and embryogenesis in the C.
772 elegans gonad by EFL-1/DPL-1 (E2F) does not require LIN-35 (pRB).
773 Development 133**:** 3147-3157.
774 Classon, M., and N. Dyson, 2001 p107 and p130: versatile proteins with interesting
775 pockets. Exp Cell Res 264**:** 135-147.
776 Classon, M., and E. Harlow, 2002 The retinoblastoma tumour suppressor in development
777 and cancer. Nat Rev Cancer 2**:** 910-917.
778 Cobrinik, D., 2005 Pocket proteins and cell cycle control. Oncogene 24**:** 2796-2809.
779 Costello, M. E., and L. N. Petrella, 2019 C. elegans synMuv B proteins regulate spatial
780 and temporal chromatin compaction during development. Development 146.
781 Cui, M., J. Chen, T. R. Myers, B. J. Hwang, P. W. Sternberg *et al.*, 2006 SynMuv genes
782 redundantly inhibit lin-3/EGF expression to prevent inappropriate vulval induction
783 in C. elegans. Dev Cell 10**:** 667-672.

784 Dick, F. A., and S. M. Rubin, 2013 Molecular mechanisms underlying RB protein function.
785 Nat Rev Mol Cell Biol 14**:** 297-306.
786 Dickinson, D. J., A. M. Pani, J. K. Heppert, C. D. Higgins and B. Goldstein, 2015
787 Streamlined Genome Engineering with a Self-Excising Drug Selection Cassette.
788 Genetics 200**:** 1035-1049.
789 Dickinson, D. J., J. D. Ward, D. J. Reiner and B. Goldstein, 2013 Engineering the
790 Caenorhabditis elegans genome using Cas9-triggered homologous
791 recombination. Nat Methods 10**:** 1028-1034.
792 Dobin, A., C. A. Davis, F. Schlesinger, J. Drenkow, C. Zaleski *et al.*, 2013 STAR: ultrafast
793 universal RNA-seq aligner. Bioinformatics 29**:** 15-21.
794 Dyson, N. J., 2016 RB1: a prototype tumor suppressor and an enigma. Genes Dev 30**:**
795 1492-1502.
796 Edelstein, A. D., M. A. Tsuchida, N. Amodaj, H. Pinkard, R. D. Vale *et al.*, 2014 Advanced
797 methods of microscope control using muManager software. J Biol Methods 1.
798 Fay, D. S., and J. Yochem, 2007 The SynMuv genes of Caenorhabditis elegans in vulval
799 development and beyond. Dev Biol 306**:** 1-9.
800 Friedland, A. E., Y. B. Tzur, K. M. Esvelt, M. P. Colaiacovo, G. M. Church *et al.*, 2013
801 Heritable genome editing in C. elegans via a CRISPR-Cas9 system. Nat Methods
802 10**:** 741-743.
803 Frokjaer-Jensen, C., M. W. Davis, C. E. Hopkins, B. J. Newman, J. M. Thummel *et al.*,
804 2008 Single-copy insertion of transgenes in Caenorhabditis elegans. Nat Genet
805 40**:** 1375-1383.

806 Gibson, D. G., L. Young, R. Y. Chuang, J. C. Venter, C. A. Hutchison, 3rd *et al.*, 2009
807 Enzymatic assembly of DNA molecules up to several hundred kilobases. Nat
808 Methods 6**:** 343-345.
809 Goetsch, P. D., J. M. Garrigues and S. Strome, 2017 Loss of the Caenorhabditis elegans
810 pocket protein LIN-35 reveals MuvB's innate function as the repressor of DREAM
811 target genes. PLoS Genet 13**:** e1007088.
812 Guiley, K. Z., A. N. Iness, S. Saini, S. Tripathi, J. S. Lipsick *et al.*, 2018 Structural
813 mechanism of Myb-MuvB assembly. Proc Natl Acad Sci U S A 115**:** 10016-10021.
814 Guiley, K. Z., T. J. Liban, J. G. Felthousen, P. Ramanan, L. Litovchick *et al.*, 2015
815 Structural mechanisms of DREAM complex assembly and regulation. Genes Dev
816 29**:** 961-974.
817 Harrison, M. M., C. J. Ceol, X. Lu and H. R. Horvitz, 2006 Some C. elegans class B
818 synthetic multivulva proteins encode a conserved LIN-35 Rb-containing complex
819 distinct from a NuRD-like complex. Proc Natl Acad Sci U S A 103**:** 16782-16787.
820 Harrison, M. M., X. Lu and H. R. Horvitz, 2007 LIN-61, one of two Caenorhabditis elegans
821 malignant-brain-tumor-repeat-containing proteins, acts with the DRM and NuRD-
822 like protein complexes in vulval development but not in certain other biological
823 processes. Genetics 176**:** 255-271.
824 Helin, K., J. A. Lees, M. Vidal, N. Dyson, E. Harlow *et al.*, 1992 A cDNA encoding a pRB-
825 binding protein with properties of the transcription factor E2F. Cell 70**:** 337-350.
826 Huang, L. S., P. Tzou and P. W. Sternberg, 1994 The lin-15 locus encodes two negative
827 regulators of Caenorhabditis elegans vulval development. Mol Biol Cell 5**:** 395-
828 411.

829 Huh, K., X. Zhou, H. Hayakawa, J. Y. Cho, T. A. Libermann *et al.*, 2007 Human
830 papillomavirus type 16 E7 oncoprotein associates with the cullin 2 ubiquitin ligase
831 complex, which contributes to degradation of the retinoblastoma tumor
832 suppressor. J Virol 81**:** 9737-9747.
833 Hurford, R. K., Jr., D. Cobrinik, M. H. Lee and N. Dyson, 1997 pRB and p107/p130 are
834 required for the regulated expression of different sets of E2F responsive genes.
835 Genes Dev 11**:** 1447-1463.
836 Irizarry, R. A., B. Hobbs, F. Collin, Y. D. Beazer-Barclay, K. J. Antonellis *et al.*, 2003
837 Exploration, normalization, and summaries of high density oligonucleotide array
838 probe level data. Biostatistics 4**:** 249-264.
839 Kim, E., L. Sun, C. V. Gabel and C. Fang-Yen, 2013 Long-term imaging of Caenorhabditis
840 elegans using nanoparticle-mediated immobilization. PLoS One 8**:** e53419.
841 Kirienko, N. V., and D. S. Fay, 2007 Transcriptome profiling of the C. elegans Rb ortholog
842 reveals diverse developmental roles. Dev Biol 305**:** 674-684.
843 Knight, A. S., M. Notaridou and R. J. Watson, 2009 A Lin-9 complex is recruited by B-
844 Myb to activate transcription of G2/M genes in undifferentiated embryonal
845 carcinoma cells. Oncogene 28**:** 1737-1747.
846 Korenjak, M., B. Taylor-Harding, U. K. Binne, J. S. Satterlee, O. Stevaux *et al.*, 2004
847 Native E2F/RBF complexes contain Myb-interacting proteins and repress
848 transcription of developmentally controlled E2F target genes. Cell 119**:** 181-193.
849 Lees, J. A., M. Saito, M. Vidal, M. Valentine, T. Look *et al.*, 1993 The retinoblastoma
850 protein binds to a family of E2F transcription factors. Mol Cell Biol 13**:** 7813-7825.

851 Lewis, P. W., E. L. Beall, T. C. Fleischer, D. Georlette, A. J. Link *et al.*, 2004 Identification
852 of a Drosophila Myb-E2F2/RBF transcriptional repressor complex. Genes Dev 18**:**
853 2929-2940.
854 Lewis, P. W., D. Sahoo, C. Geng, M. Bell, J. S. Lipsick *et al.*, 2012 Drosophila lin-52 acts
855 in opposition to repressive components of the Myb-MuvB/dREAM complex. Mol
856 Cell Biol 32**:** 3218-3227.
857 Liban, T. J., E. M. Medina, S. Tripathi, S. Sengupta, R. W. Henry *et al.*, 2017 Conservation
858 and divergence of C-terminal domain structure in the retinoblastoma protein family.
859 Proc Natl Acad Sci U S A 114**:** 4942-4947.
860 Liban, T. J., M. J. Thwaites, F. A. Dick and S. M. Rubin, 2016 Structural Conservation
861 and E2F Binding Specificity within the Retinoblastoma Pocket Protein Family. J
862 Mol Biol 428**:** 3960-3971.
863 Litovchick, L., L. A. Florens, S. K. Swanson, M. P. Washburn and J. A. DeCaprio, 2011
864 DYRK1A protein kinase promotes quiescence and senescence through DREAM
865 complex assembly. Genes Dev 25**:** 801-813.
866 Litovchick, L., S. Sadasivam, L. Florens, X. Zhu, S. K. Swanson *et al.*, 2007 Evolutionarily
867 conserved multisubunit RBL2/p130 and E2F4 protein complex represses human
868 cell cycle-dependent genes in quiescence. Mol Cell 26**:** 539-551.
869 Love, M. I., W. Huber and S. Anders, 2014 Moderated estimation of fold change and
870 dispersion for RNA-seq data with DESeq2. Genome Biol 15**:** 550.
871 Lu, X., and H. R. Horvitz, 1998 lin-35 and lin-53, two genes that antagonize a C. elegans
872 Ras pathway, encode proteins similar to Rb and its binding protein RbAp48. Cell
873 95**:** 981-991.

874 Mages, C. F., A. Wintsche, S. H. Bernhart and G. A. Muller, 2017 The DREAM complex
875 through its subunit Lin37 cooperates with Rb to initiate quiescence. Elife 6.
876 Marceau, A. H., J. G. Felthousen, P. D. Goetsch, A. N. Iness, H. W. Lee *et al.*, 2016
877 Structural basis for LIN54 recognition of CHR elements in cell cycle-regulated
878 promoters. Nat Commun 7**:** 12301.
879 Marnik, E. A., J. H. Fuqua, C. S. Sharp, J. D. Rochester, E. L. Xu *et al.*, 2019 Germline
880 Maintenance Through the Multifaceted Activities of GLH/Vasa in Caenorhabditis
881 elegans P Granules. Genetics 213**:** 923-939.
882 Muller, G. A., and K. Engeland, 2010 The central role of CDE/CHR promoter elements in
883 the regulation of cell cycle-dependent gene transcription. FEBS J 277**:** 877-893.
884 Muller, G. A., M. Quaas, M. Schumann, E. Krause, M. Padi *et al.*, 2012 The CHR promoter
885 element controls cell cycle-dependent gene transcription and binds the DREAM
886 and MMB complexes. Nucleic Acids Res 40**:** 1561-1578.
887 Muller, G. A., K. Stangner, T. Schmitt, A. Wintsche and K. Engeland, 2017 Timing of
888 transcription during the cell cycle: Protein complexes binding to E2F, E2F/CLE,
889 CDE/CHR, or CHR promoter elements define early and late cell cycle gene
890 expression. Oncotarget 8**:** 97736-97748.
891 Myers, T. R., and I. Greenwald, 2005 lin-35 Rb acts in the major hypodermis to oppose
892 ras-mediated vulval induction in C. elegans. Dev Cell 8**:** 117-123.
893 Narasimha, A. M., M. Kaulich, G. S. Shapiro, Y. J. Choi, P. Sicinski *et al.*, 2014 Cyclin D
894 activates the Rb tumor suppressor by mono-phosphorylation. Elife 3.

895 Osterloh, L., B. von Eyss, F. Schmit, L. Rein, D. Hubner *et al.*, 2007 The human synMuv-
896 like protein LIN-9 is required for transcription of G2/M genes and for entry into
897 mitosis. EMBO J 26**:** 144-157.
898 Pang, C. L., S. Y. Toh, P. He, S. Teissier, Y. Ben Khalifa *et al.*, 2014 A functional
899 interaction of E7 with B-Myb-MuvB complex promotes acute cooperative
900 transcriptional activation of both S- and M-phase genes. (129 c). Oncogene 33**:**
901 4039-4049.
902 Petrella, L. N., W. Wang, C. A. Spike, A. Rechtsteiner, V. Reinke *et al.*, 2011 synMuv B
903 proteins antagonize germline fate in the intestine and ensure C. elegans survival.
904 Development 138**:** 1069-1079.
905 Pilkinton, M., R. Sandoval and O. R. Colamonici, 2007 Mammalian Mip/LIN-9 interacts
906 with either the p107, p130/E2F4 repressor complex or B-Myb in a cell cycle-phase-
907 dependent context distinct from the Drosophila dREAM complex. Oncogene 26**:**
908 7535-7543.
909 Rechtsteiner, A., M. E. Costello, T. A. Egelhofer, J. M. Garrigues, S. Strome *et al.*, 2019
910 Repression of Germline Genes in Caenorhabditis elegans Somatic Tissues by
911 H3K9 Dimethylation of Their Promoters. Genetics 212**:** 125-140.
912 Rubin, S. M., 2013 Deciphering the retinoblastoma protein phosphorylation code. Trends
913 Biochem Sci 38**:** 12-19.
914 Sadasivam, S., S. Duan and J. A. DeCaprio, 2012 The MuvB complex sequentially
915 recruits B-Myb and FoxM1 to promote mitotic gene expression. Genes Dev 26**:**
916 474-489.

917 Saffer, A. M., D. H. Kim, A. van Oudenaarden and H. R. Horvitz, 2011 The Caenorhabditis
918 elegans synthetic multivulva genes prevent ras pathway activation by tightly
919 repressing global ectopic expression of lin-3 EGF. PLoS Genet 7**:** e1002418.
920 Schmit, F., S. Cremer and S. Gaubatz, 2009 LIN54 is an essential core subunit of the
921 DREAM/LINC complex that binds to the cdc2 promoter in a sequence-specific
922 manner. FEBS J 276**:** 5703-5716.
923 Schmit, F., M. Korenjak, M. Mannefeld, K. Schmitt, C. Franke *et al.*, 2007 LINC, a human
924 complex that is related to pRB-containing complexes in invertebrates regulates the
925 expression of G2/M genes. Cell Cycle 6**:** 1903-1913.
926 Schneider, C. A., W. S. Rasband and K. W. Eliceiri, 2012 NIH Image to ImageJ: 25 years
927 of image analysis. Nat Methods 9**:** 671-675.
928 Tabuchi, T. M., B. Deplancke, N. Osato, L. J. Zhu, M. I. Barrasa *et al.*, 2011 Chromosome-
929 biased binding and gene regulation by the Caenorhabditis elegans DRM complex.
930 PLoS Genet 7**:** e1002074.
931 Tao, Y., R. F. Kassatly, W. D. Cress and J. M. Horowitz, 1997 Subunit composition
932 determines E2F DNA-binding site specificity. Mol Cell Biol 17**:** 6994-7007.
933 Tedesco, D., J. Lukas and S. I. Reed, 2002 The pRb-related protein p130 is regulated by
934 phosphorylation-dependent proteolysis via the protein-ubiquitin ligase SCF(Skp2).
935 Genes Dev 16**:** 2946-2957.
936 Vorster, P. J., P. Goetsch, T. U. Wijeratne, K. Z. Guiley, L. Andrejka *et al.*, 2020 A long
937 lost key opens an ancient lock: Drosophila Myb causes a synthetic multivulval
938 phenotype in nematodes. Biol Open 9.

939 Wang, D., S. Kennedy, D. Conte, Jr., J. K. Kim, H. W. Gabel *et al.*, 2005 Somatic
940 misexpression of germline P granules and enhanced RNA interference in
941 retinoblastoma pathway mutants. Nature 436**:** 593-597.
942 Zhang, B., W. Chen and A. Roman, 2006 The E7 proteins of low- and high-risk human
943 papillomaviruses share the ability to target the pRB family member p130 for
944 degradation. Proc Natl Acad Sci U S A 103**:** 437-442.
945 Zwicker, J., F. C. Lucibello, L. A. Wolfraim, C. Gross, M. Truss *et al.*, 1995 Cell cycle
946 regulation of the cyclin A, cdc25C and cdc2 genes is based on a common
947 mechanism of transcriptional repression. EMBO J 14**:** 4514-4522.

948